Available online at www.sciencedirect.com
SCIENCE DIRECT®
Journal of Magnetic Resonance 163 (2003) 73–80
JMR Journal of Magnetic Resonance
www.elsevier.com/locate/jmr

Slice-selective *J*-coupled coherence transfer using symmetric linear phase pulses: applications to localized GABA spectroscopy

Jun Shen*

Molecular Imaging Branch, Mood and Anxiety Disorders Program, National Institute of Mental Health, Rm. 2D51A, Bldg. 10, 9000 Rockville Pike, MSC 1527, Bethesda, MD 20892-1527, USA

Received 2 December 2002; revised 19 March 2003

Abstract

Symmetric, linear phase, slice-selective RF pulses were analyzed theoretically for performing slice-selective coherence transfer. It was shown using numerical simulations of product operators that, when a prefocusing gradient of the same area as that of the refocusing gradient is added, these pulses become slice-selective universal rotator pulses, therefore, capable of performing slice-selective coherence transfer. As an example, a slice-selective universal rotator pulse based on a seven-lobe hamming-filtered sinc pulse was applied to in vivo single-shot simultaneous spectral editing and spatial localization of neurotransmitter GABA in the human brain.
Published by Elsevier Science (USA).

Keywords: Rotator symmetry; Spectral editing; Spatial localization; GABA; In vivo magnetic resonance spectroscopy

1. Introduction

Selective pulses have found widespread applications in both high-resolution NMR spectroscopy and in in vivo imaging and localized spectroscopy [1,2]. A unique class of shaped pulses generally referred to as selective universal rotator pulses [3] perform well-defined spin rotations within the selected frequency range regardless of the initial state of the magnetization. In high-resolution NMR spectroscopy these selective universal rotator pulses have been used in a variety of selective coherence transfer applications (e.g. [3–5]). In contrast, in in vivo localized spectroscopy applications, use of selective pulses is usually limited to spatially and/or spectrally selective excitation, inversion and refocusing. When a pulse is needed for conversion of multiple quantum coherences or for polarization transfer in localized spectroscopy a nonselective hard pulse is usually used (e.g. [6–9]). The necessity of using spatially nonselective pulses in localized spectroscopy limits the options of spatial localization and also may increase the difficulty of outer volume suppression. Since selective universal rotator pulses are equivalents of hard pulses in the selected frequency range it is desirable to use them to achieve spatially selective coherence transfer.

The conventional selective universal rotator pulses designed for high-resolution NMR spectroscopy [3–5] suffer from high peak RF power requirement when used in in vivo localized spectroscopy which is often performed on much lower field strength spectrometers using much larger RF transmit coils. In addition, these pulses require high B_1 homogeneity [3] which is very difficult to achieve in in vivo spectroscopy experiments. However, it has been recognized for some time in the field of magnetic resonance imaging that symmetric, linear phase, slice-selective RF pulses such as sinc pulses, which are based on the linear response theory, and the linear phase SLR pulses [10] act on nonequilibrium magnetization as hard pulses within the selected slice when a prefocusing gradient pulse of the same area as that of the refocusing one is added [11]. For example, in an excellent fat suppression scheme [12,13], slice-selective pulse trains were used in a spatially and spectrally selective fashion to minimize excitation of fat from the

* Fax: 1-301-480-2397.
E-mail address: shenj@intra.nimh.nih.gov.

1090-7807/03/$ - see front matter. Published by Elsevier Science (USA).
doi:10.1016/S1090-7807(03)00112-5

selected slice. In the slice-selective pulse trains each RF component of a conventional semi-selective pulse train was replaced by a short slice-selective sinc pulse, which was flanked by a pair of prefocusing and refocusing gradient pulses to allow it to behave like a slice-selective universal rotator pulse.

In this paper we demonstrate that symmetric, linear phase, slice-selective pulses can also be used to perform slice-selective coherence transfer such as polarization transfer and conversion of multiple quantum states. Their relatively low RF power requirement and/or shorter pulse duration as well as high resistance to degradation of selectivity caused by B_1 inhomogeneity makes them ideal candidates for localized spectroscopy applications. A general theoretical description of the pulses is given here to facilitate discussion of their applications to slice-selective coherence transfer. The application of these pulses to in vivo single-shot localized detection of neurotransmitter GABA in the human brain is demonstrated experimentally.

2. Results

It has been proven that for any time-symmetric rotation along the x-axis the overall rotation axis at each offset is confined to the xz plane [14]. If a time-symmetric selective RF pulse rotates the equilibrium magnetization by the same angle θ onto the yz plane within its bandwidth then this time-symmetric RF pulse is a selective universal rotator pulse along the x-axis with a flip angle of θ for each offset within its bandwidth [3,14]. In the case of a sinc or other symmetric and linear phase pulses, addition of a prefocusing gradient pulse of the same area as that of the refocusing one, therefore, converts the pulse into a spatially selective universal rotator pulse while ignoring the evolution of chemical shift and B_0 inhomogeneity during the RF-gradient pulse scheme.

To illustrate the properties of the overall propagator of the slice selective universal rotator pulses we use the formalism of quaternion analysis [4,15]. For an ideal symmetric, linear phase, selective pulse applied along the x-axis with a uniform passband the results are listed in Table 1 which describes the properties of the propagator within the passband for each component of the RF-gradient pulse scheme. The quaternion elements of the overall RF-gradient propagator within the passband indicate a pure phase and uniform rotation by an angle θ along the x-axis. Note that θ is also the flip angle of the RF-gradient pulse scheme.

Fig. 1 shows results of numerical simulation of the overall quaternion elements of a 90° 1.5 ms hamming-filtered seven-lobe sinc pulse configured as a slice-selective universal rotator pulse. The strength of the slice selection gradient used is 1 G/cm. The areas of the prefocusing and refocusing gradient pulses are 50% of that of the slice-selection gradient pulse. As seen in Fig. 1, within the selected slice a relatively pure phase and uniform 90° rotation is obtained as quaternion elements—$A \approx D \approx \frac{1}{\sqrt{2}}$; and $B \approx C \approx 0$ across the passband of the slice. Although not shown in the simulations here it should be noted that due to deviation from the linear response theory a slightly larger area of prefocusing and refocusing gradient pulses than the theoretical 50% of that of the slice-selective gradient would be required to obtain a pure phase within the selected slice [2]. Deviation from the linear response theory at large flip angles ($\theta > 90°$) also causes degradation of the selectivity of the pulse.

Fig. 2 compares simulated spatial profiles of the IS spin system polarization transfer yield and the double quantum yield using the 90° slice-selective universal rotator RF-gradient pulse scheme described above. For polarization transfer, a 90° hard pulse along the y axis converts the antiphase magnetization $2I_xS_z$ into $2I_zS_x$ with 100% yield. The spatial profile of polarization transfer generated by the proposed 90° slice-selective universal rotator RF-gradient pulse scheme can be obtained by numerically integrating the Bloch equation for I_x and S_z, respectively. The polarization transfer yield is then the product of that of I_z and S_x. Similarly, for double quantum coherence preparation, a 90° hard pulse along the x axis converts the antiphase magnetization $2I_xS_z + 2I_zS_x$ into $2I_xS_y + 2I_yS_x (= \mathrm{DQC}_y)$ with 100% yield. The spatial profile of double quantum coherence generated by the proposed 90° slice-selective universal rotator RF-gradient pulse scheme can be obtained by numerically integrating the Bloch equation for I_x, I_z, S_x, and S_z, respectively. The double quantum yield can then be calculated based on its expression in terms

Table 1
Passband quaternion elements of a uniform, pure phase, slice-selective universal rotator pulse based on a symmetric, linear phase, selective RF pulse

Quaternion elements	A	B	C	D
Prefocusing gradient	0	0	$-\sin(\frac{\alpha}{2})$	$\cos(\frac{\alpha}{2})$
RF and slice gradient	$-\sin(\frac{\theta}{2})$	0	$\sin(\alpha)\cos(\frac{\theta}{2})$	$\cos(\alpha)\cos(\frac{\theta}{2})$
Refocusing gradient	0	0	$-\sin(\frac{\alpha}{2})$	$\cos(\frac{\alpha}{2})$
Universal rotator pulse	$-\sin(\frac{\theta}{2})$	0	0	$\cos(\frac{\theta}{2})$

$\alpha(\mathbf{r}) = \int_0^\tau \mathbf{G}\cdot\mathbf{r}\,dt$, τ is the duration of slice-selection gradient pulse, θ is the flip angle of the selective RF pulse. $A \equiv l_{xx}\cos(\delta/2)$; $B \equiv l_{yy}\cos(\delta/2)$; $C \equiv l_{zz}\cos(\delta/2)$; $D \equiv \sin(\delta/2)$ where l_{xx}, l_{yy}, and l_{zz} are directional cosines and δ the angle of rotation around an axis defined by l_{xx}, l_{yy}, and l_{zz}.

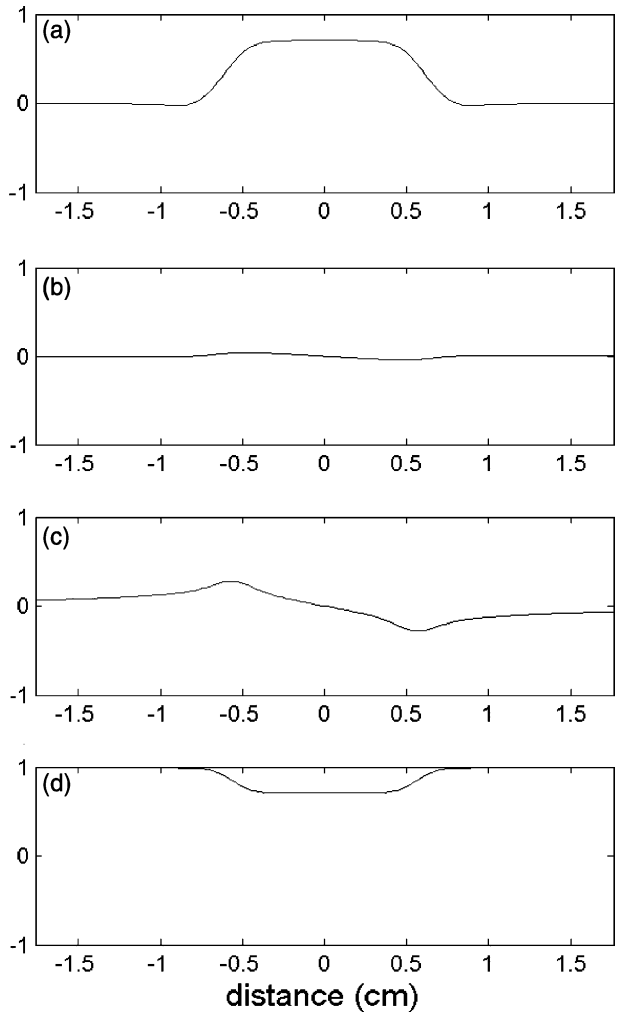

Fig. 1. Quaternion elements of a 90° 1.5 ms hamming-filtered seven-lobe sinc pulse configured as a slice-selective universal rotator pulse with the areas of the prefocusing and refocusing gradients set to 50% of that of the slice-selection gradient. The slice-selection gradient is 1 G/cm in all cases. From top to bottom: quaternion element – A; quaternion element B; quaternion element C; and quaternion element D.

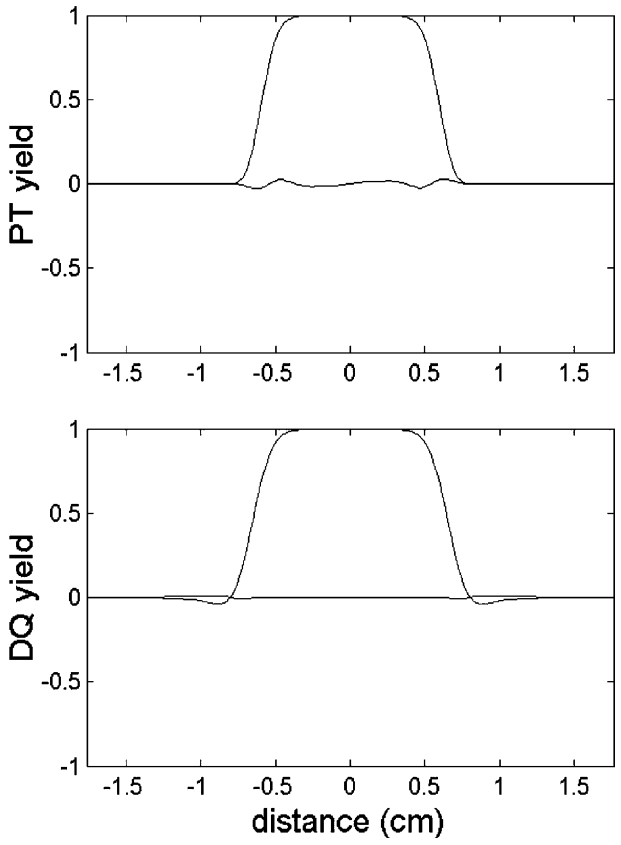

Fig. 2. Spatial profiles of polarization transfer (PT) and double quantum (DQ) yields of the 90° pulse described in Fig. 1. For polarization transfer, $2I_yS_z \rightarrow 2I_zS_y$; for double quantum preparation, $2I_xS_z + 2I_zS_x \rightarrow \mathrm{DQC}_y$. Top: polarization transfer; Bottom: double quantum preparation. The slice-selection gradient is 1 G/cm in both cases. The dispersive components are I_zS_x in polarization transfer and DQC_x in double quantum preparation, respectively. Note that the areas of the prefocusing and refocusing gradient lobes of the hamming-filtered seven lobe sinc pulse were set to an empirically optimized 51.1% of that of the slice selection gradient.

of product operators. For $2I_xS_z \rightarrow 2I_zS_x$ and $2I_xS_z + 2I_zS_x \rightarrow \mathrm{DQC}_y$, $\sim 100\%$ polarization transfer yield and double quantum yield are obtained respectively within the passband of the pulse using the slice-selective universal rotator pulse as shown in Fig. 2.

For a direct visualization of localization by the proposed slice-selective coherence transfer scheme a phantom containing 99% isopropanol was used. The one-dimensional images of the methyl group were obtained with and without the slice-selective universal rotator pulse. Fig. 3(a) shows the double quantum filtered isopropanol spectrum using a standard non-selective double quantum sequence (see Fig. 1(c) in [16]). Fig. 3(b) shows the y projection image of the phantom sample using the same sequence except that the FID mode was switched to one-dimensional imaging mode. In Fig. 3(c) the second nonselective 90° pulse in the double quantum sequence which converts the antiphase magnetization into double quantum coherence was replaced by the proposed slice-selective universal rotator pulse scheme. The resultant y projection image in Fig. 3(c) shows that coherence transfer was localized to the selected slice. In addition, variation of the double quantum yield for off-centered slices was demonstrated by shifting the frequency of the slice-selective coherence transfer pulse relative to the resonance frequency of the methyl group at 1.16 ppm. The dependence of the signal magnitude of the double quantum filtered methyl group on the frequency offset of the slice-selective universal rotator pulse is shown in Fig. 3(d).

The spatially selective universal rotator pulse was applied here to in vivo GABA editing in the human brain. The GABA editing pulse sequence depicted in Fig. 4 was modified from a previously published method [17] which uses a doubly selective multiple quantum filter and three-dimensional ISIS localization for GABA

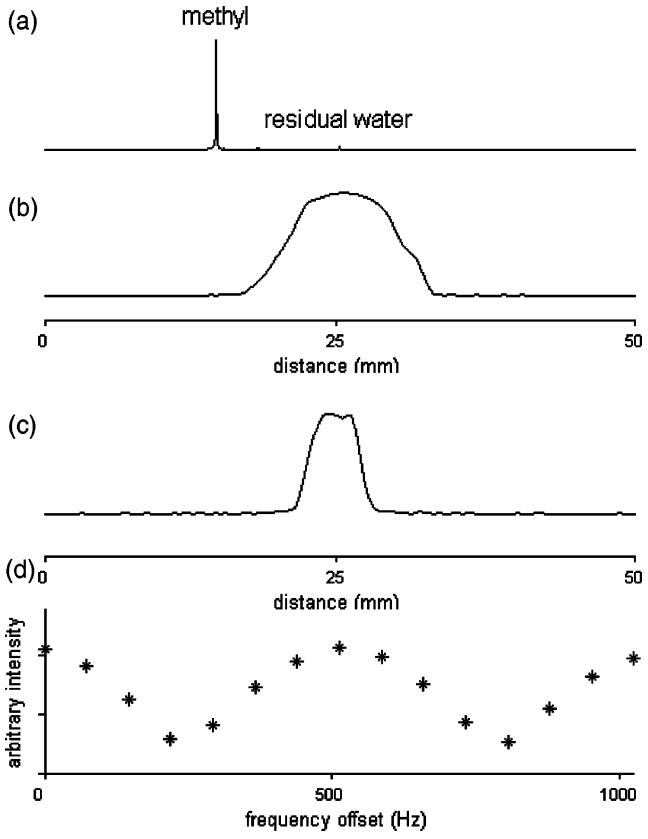

Fig. 3. (a) Spectrum of double quantum filtered isopropanol using the pulse sequence described in Fig. 1(c) [16]. The spectrally selective 90° pulse was placed on the methyl group. All pulses were spatially nonselective. (b) The one-dimensional projection of the phantom generated by the double quantum filtered methyl group. (c) Same as in (b) except that the second nonselective 90° pulse in the double quantum sequence was replaced by a 1.5 ms seven-lobe sinc pulse configured into a slice-selective coherence transfer pulse centered at the gradient isocenter. Slice thickness = 4.5 mm. (d) The magnitude of the double quantum filtered methyl group as a function of the frequency offset of the slice-selective coherence transfer pulse using the pulse sequence described in (c) except that the FID mode was used. All experiments were performed on an 11.7 T Bruker AVANCE spectrometer using a 3.5 cm ID volume coil and a 1.5 cm diameter spherical phantom containing 99% isopropanol.

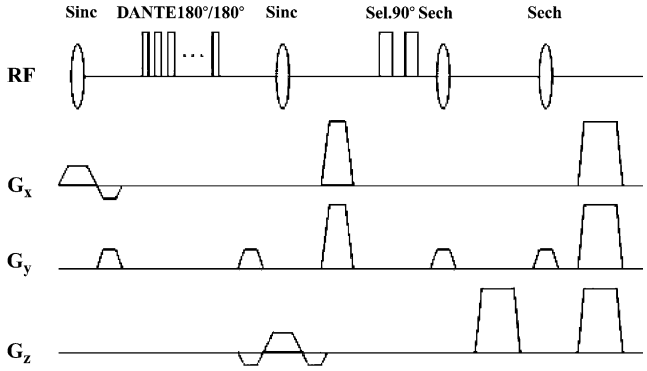

Fig. 4. GABA editing pulse sequence using a slice-selective universal rotator pulse for multiple quantum editing of GABA at 3.0 ppm. The phases of the odd-numbered RF components in the doubly selective DANTE pulse train were set to 0° while those of the even-numbered components were linearly incremented in the step of 90° [17]. The overall phase of the even-numbered RF components was also set to 0°. The inter-pulse delay between the odd- and between the even-numbered pulses is approximately $0.25/|\upsilon_{\text{GABA-4}} - \upsilon_{\text{GABA-3}}|$. The second 90° pulse is the slice-selective universal rotator pulse which converts the antiphase coherences into GABA-3 and -4 double quantum coherence. The multiple quantum preparation scheme is preceded by three CHESS pulses for water suppression, and then outer-volume suppression (OVS) along $-x$, x, $-y$, y, $-z$ and z directions. The CHESS and OVS schemes were not drawn for clarity. Immediately after the multiple quantum preparation, the double quantum coherence is encoded by two 4 ms, 1.4 G/cm gradient pulses along x- and y-axes. The duration of the double quantum filtering gradients is 8 ms with the same strength as the double quantum encoding gradients.

measurement. The first 90° pulse, the doubly selective 180° DANTE refocusing pulse [18] on GABA-3 and GABA-4, and the second 90° pulse selectively prepare the GABA-3 and -4 double quantum coherence. To achieve simultaneous spatial localization and spectral editing in each single shot the first 90° hard pulse for excitation of equilibrium magnetization in the original pulse sequence was replaced by a 1.5 ms 90° seven-lobe sinc pulse to select an x slice. The second 90° hard pulse for conversion of antiphase single quantum coherence into double quantum coherence was replaced by the same 90° pulse configured as a universal rotator pulse with gradient pulses along the z direction. After gradient labeling the double quantum coherence is converted into antiphase GABA-4 single quantum coherence. The hard 180° pulse for rephasing the GABA-4 antiphase doublet was replaced by a pair of identical 3.5 ms hyperbolic secant pulses ($\mu = 5$, 1% truncation) for slice-selective refocusing along the y direction [19].

Fig. 5 shows the in vivo spectra with TE = 68 ms from a $4 \times 2 \times 3$ cm^3 voxel in the occipital lobe of a healthy adult volunteer. First, the unedited spin-echo spectrum (top trace) was acquired with NS = 8. A 4-Hz line broadening was used for post-acquisition processing. Then GABA editing pulse sequence depicted in Fig. 4 was applied to the same voxel. The edited spectrum (bottom trace) was acquired with 128 scans. The same post-acquisition line broadening was applied. The doubly selective double quantum filter suppressed the dominant creatine singlet at 3.0 ppm and revealed the underneath GABA-4 doublet at 3.0 ppm. The doubly selective double quantum filter also suppresses other singlets and coupled spins such as choline-containing compounds, NAA, glutathione, macromolecules, glutamate, and glutamine [17,20].

3. Discussion

For simplicity, the areas of the prefocusing and refocusing gradient lobes of the slice-selective universal rotator pulses were set to 50% of that of the slice

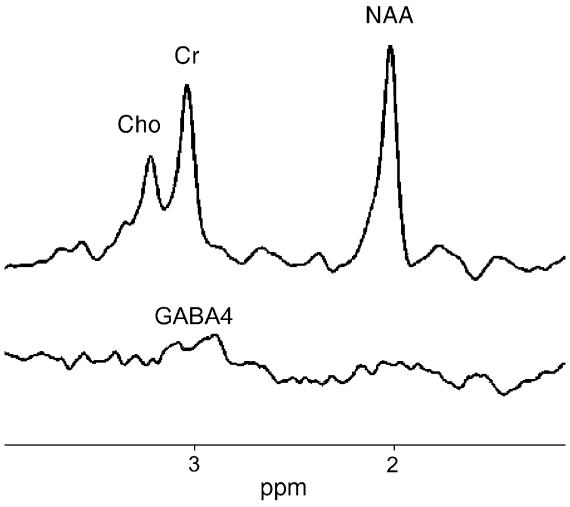

Fig. 5. The sequence shown in Fig. 4 was tested on a Bruker AVANCE 2.1 T whole-body spectrometer using an 8-cm diameter surface coil placed directly under the occipital lobe of an adult healthy volunteer. The B_0 homogeneity was optimized using the FASTERMAP method [29] to correct all first- and second-order shims automatically. A three slice (coronal, axial, and sagittal) gradient echo imaging method was used for positioning of the subject. The localized volume is $4 \times 2 \times 3$ cm^3 placed in the occipital lobe and approximately 2-cm deep from the dura. RF pulse power was accurately calibrated using a two-dimensional STEAM method localizing a y column through the center of the voxel by placing the 180° null generated by the first RF pulse of the STEAM sequence at the center of the localized voxel. Top trace: in vivo unedited spin-echo spectrum with TE = 68 ms from the $4 \times 2 \times 3$ cm^3 voxel. Eight scans were acquired with 4-Hz post-acquisition line broadening. The 3.0 ppm resonance is dominated by the single quantum methyl protons from creatine; Bottom trace: In vivo double quantum edited spectrum using the pulse sequence shown in Fig. 4 from the same voxel. One hundred and twenty eight scans were acquired with 4 Hz post-acquisition line broadening. The dominant creatine methyl protons at 3.0 ppm (along with NAA at 2.0 ppm and choline-containing compounds at 3.2 ppm) were suppressed, revealing the underneath GABA-4 signal at 3.0 ppm.

selection gradient in the numerical simulations shown in Fig. 1. Due to deviation from the linear response theory, the actual areas of the prefocusing and refocusing gradient lobes for a sinc pulse is slightly greater than the theoretical 50%. As a result, transverse spins outside the selected slice (i.e., in the stopband) experience a small net dephasing gradient in addition to the transient Bloch–Siegert effect [21]. For localized spectroscopy applications, the small net dephasing effect on the stopband (outer volume) transverse magnetization is of no significance. For transverse spins inside the slice, the correct prefocusing and refocusing gradients lead to an improved spatial profile both in numerical simulations and in experimental tests. Fig. 2 shows the spatial profiles of polarization transfer yield and double quantum coherence yield when the areas of the prefocusing and refocusing gradient lobes of the hamming-filtered seven lobe sinc pulse were set to an empirically optimized 51.1% of that of the slice selection gradient. The dispersive components caused by the quaternion element C in Fig. 1 are largely absent in Fig. 2 when the prefocusing and refocusing gradient areas are set to 51.1% of that of the slice selection gradient. It should also be pointed out, however, that the exact optimal prefocusing and refocusing gradient areas depend on the type and flip angle of a specific symmetric and linear phase RF pulse.

Although only slice-selective universal rotator sinc pulses are demonstrated here the general configuration is obviously applicable to all symmetric, linear phase, selective RF pulses including those based on the linear response theory. For example, Gaussian [22], Hermite [23], and the linear phase SLR [10] pulses can be configured into slice-selective universal rotator pulses although the Gaussian and Hermite pulses do not generate a "top hat" excitation profile. Compared to 90° U-BURP [3] and Q5 [4] pulses, which require no prefocusing or refocusing gradients (except those for compensating the rising and falling edges of the slice selection gradient), the linear phase pulses generally require much less peak RF power (see Table 2), therefore, are particularly suitable for many in vivo applications when large volume coils are necessary. For not very large flip angles ($\theta \leqslant 90°$) the linear response theory based pulses can be set to arbitrary flip angles. Also, B_1 inhomogeneity has negligible effects on the integrity (selectivity, phase, and uniformity) of the excitation profile of these pulses provided that the nominal flip angle is not very large. In contrast, the integrity of the prefocused universal rotator pulses such as the U-BURP and Q5 pulses degrades significantly at the presence of ca. 5–10% or greater B_1 inhomogeneity.

The advantage of the slice-selective pulses over the equivalent non-selective "hard" pulses in localized spectroscopy is that the slice-selective pulses minimize excitation of outer volume magnetization. As in any other schemes of localizing transverse spins, the slice-selective coherence or polarization transfer pulses alone do not necessarily provide adequate localization unless

Table 2
Comparison of slice-selective 90° universal rotator pulses: pulse duration and peak RF amplitude requirements

RF pulses	$\Delta\omega * T$[a]	A[b]
U-BURP [3]	4.9	42.6
Q5 [4]	6.1	19.3
Linear phase SLR [8][c]	6.4	6.2
7-lobe Sinc	7.9	8.5
Hamming-filtered 7-lobe sinc	8.2	8.1
5-Lobe sinc	6.0	5.7
Hamming-filtered 5-lobe sinc	6.3	6.0

[a] $\Delta\omega$ denotes the bandwidth of excitation profile of the pulse at half-height. $\Delta\omega * T$ is a dimensionless constant.

[b] A denotes the ratio of the peak amplitude of the pulse to that of a 90° rectangular pulse of the same duration.

[c] Passband ripple: 1%; stopband ripple: 1%; digitization steps: 128.

crasher gradients associated with the slice-selective universal rotator pulses are used. The crusher gradients, however, often reduce the yield of coherence or polarization transfer (e.g. [24]). Fortunately, numerous opportunities exist for the effective application of the slice-selective universal rotator pulses. In fat suppressed water imaging applications [12,13], only spins within the selected slice(s) need to be acted on by the slice-selective universal rotator pulses. In localized spectroscopy, however, three orthogonal slices are excited for localization of a single voxel. For example, in the localized SUPERCOSY experiment [7] localization is provided by the first 90° pulse and the two 180° refocusing pulses which are orthogonal to the 90° pulse and to each other. A slice-selective universal rotator 90° pulse could be used to replace the hard non-selective 90° pulse for localized polarization transfer while avoiding excitation of the entire volume. When applied to double-quantum filtered spectroscopy experiments the double quantum filter gradients act as the crasher gradient for the slice-selective universal rotator pulse(s). In the case of GABA editing shown in Fig. 4, the first 90° pulse excites the x slice. The second 90° pulse, acting as a slice-selective universal rotator pulse along the z axis, converts the antiphase spins at the intersection of the two slices into the GABA-3 and -4 double quantum coherence. The transverse spins from the x and z slices but outside the y column at their intersection are dephased, in part, by the double quantum filter gradients.

In our previous GABA editing method using a doubly selective DANTE refocusing pulse for selective preparation of GABA-3 and -4 double quantum [17] spatial localization was achieved using the 8-step three-dimensional ISIS method. In this sequence, only the first 90° pulse and the second 180° pulse are available for conventional spatial localization because the doubly selective DANTE pulse is necessary to effectively suppress overlapping glutathione and mobile macromolecules around 3.0 ppm [20]. As discussed above, localization of the transverse spins via the slice-selective universal rotator pulse in Fig. 4 has made it feasible to achieve simultaneous spectral editing and three-dimensional spatial localization of GABA in a single shot using the doubly selective DANTE method. Due to the low GABA concentration in the human brain [25,26] long signal averaging is still indispensable for any meaningful GABA measurement. Nevertheless, the new single-shot GABA method proposed here and previously published single-shot methods [9,20] eliminate ISIS subtraction errors due to potential patient movement and instrumental instability. As demonstrated in Fig. 5 the slice-selective universal rotator pulses based on symmetric and linear phases pulses can be used to obtain single-shot simultaneous spectral editing and spatial localization of GABA in the brain while using the doubly selective DANTE pulse for double quantum preparation to ensure clean editing. As described previously [17] when spectrally non-selective 180° pulse is used in DQ preparation (e.g., [9,19,20]), suppression of contaminating J-coupled signals at 3.0 ppm depends on the spectral selectivity of the selective 90° pulse which converts GABA-3 and -4 DQC_y into GABA-4 antiphase coherence (i.e., the third 90° pulse). Significant improvements in spectral selectivity have been achieved using the doubly selective DANTE pulse approach which completely eliminates interfering glutathione resonances and dramatically reduced contamination from signals generated by mobile macromolecules [17]. The doubly selective DANTE pulse also refocuses the GABA-2 and -3 J evolution during the DQ preparation leading to a theoretical 33% increase in double quantum yield as compared to DQ GABA editing methods using spectrally non-selective 180° pulse in DQ preparation (e.g. [9,19,20]).

In contrast to the equivalent non-selective "hard" pulses in localized spectroscopy the slice-selective universal rotator pulses are affected by the well-known chemical shift artefact which causes a displacement of the selected slice depending on the chemical shift of the resonance of interest. As demonstrated recently [27,28], in localized spectroscopy of coupled spins the chemical shift artifact could also lead to a significant loss of signal and corruption of the slice profile due to the regions where only one of the two coupled spins is acted on by the slice-selective pulses. A detailed product operator analysis of this effect was performed for the pulse sequence depicted in Fig. 4. The product operator terms generated by the 90° slice-selective universal rotator pulse in different regions were tabulated in Table 3. In the center where the two $I+S$ regions intercept each other, both pulses excite the two coupled spins. The

Table 3
Product operator terms generated by the 90° slice-selective universal rotator pulse in Fig. 4

2nd slice-sel. 90° pulse \ 1st slice-sel. 90° pulse	I	I+S	S
I	$2I_xS_z$	$2I_yS_x$	$2I_yS_x$
I+S	$2I_xS_y$	$2I_xS_y+2I_yS_x$	$2I_yS_x$
S	$2I_xS_y$	$2I_xS_y$	$2I_zS_x$

I, $I+S$, and S denote regions where only the I spin, both the I and the S spins, or only the S spin are excited.

desired double quantum terms are generated there. In regions where only one of the two product operator terms in DQC_y is generated, the double quantum yield is only 50% of that in the center. In regions where anti-phase single quantum coherences are generated, the double quantum yield is zero. Therefore, in situations where a volume coil is used, for example, the chemical shift effects can be significantly detrimental for methods based on slice-selective DQ filtering [28]. Fortunately, the bandwidths of the slice-selective pulses used in the GABA editing sequence are 5467 Hz for the sinc pulses and 5171 Hz for the sech pulse, respectively. The chemical shift difference between GABA-3 and GABA-4 resonance is 98 Hz. The slice displacement due to chemical shift using our GABA editing sequence is less than 2% of the slice thickness, therefore, its effect on the GABA measurement presented here is negligible.

As illustrated previously [8,9], when the first 90° and/or the first 180° spatially nonselective pulse in a double quantum sequence are replaced by off-centered slice-selective pulses the accompanying frequency switches disrupt the phase coherence of the transverse magnetization during double quantum preparation. As a result, the double quantum yield becomes dependent on the frequency offset (or, equivalently, on the position of the off-centered slice) if the phase of the second 90° pulse remains on the x axis. Since only the difference between the phase of the transverse magnetization and that of the second 90° pulse matters we expect the same effect when the second 90° pulse is also made an off-centered slice-selective one. This was verified in Fig. 3(d) where the double quantum yield of isopropanol was found to be a sinusoidal function of the frequency offset of the slice-selective universal rotator pulse as expected. For in vivo GABA editing, only the voxel at the gradient isocenter was used. If the voxel needs to be placed off-center the phase of the second 90° pulse, i.e., the slice selective universal rotator pulse needs to be pre-calibrated for different voxel locations to ensure maximum double quantum yield just as in the case when a nonselective hard pulse was used [9] or the voxel must be placed at discrete locations to achieve maximum signal intensity when the second 90° pulse remained at the x axis [8].

4. Conclusions

We have shown that slice-selective universal rotator pulses based on symmetric, linear phase RF pulses can be used for slice-selective J-coupled coherence transfer in localized spectroscopy. In comparison to prefocused universal rotator pulses, these pulses require significantly low B_1 homogeneity, low RF peak power and/or short pulse duration when used for spatial localization and simultaneous coherence transfer. They can be used to replace non-selective hard pulses for slice-selective coherence transfer, e.g., in in vivo single-shot simultaneous spectral editing and spatial localization of neurotransmitter GABA in the human brain.

Acknowledgments

The author thanks Dr. Alan Koretsky for permission to use the 11.7 T spectrometer; Drs. Zhengguang Chen, Douglas L. Rothman, and In-Young Choi for helpful discussions; and the anonymous reviewers for valuable comments.

References

[1] R. Freeman, Selective excitation in high-resolution NMR, Chem. Rev. 91 (1991) 1397–1412.
[2] E.M. Haacke, R.W. Brown, M.R. Thompson, R. Venkatesan, Magnetic Resonance Imaging, Physical Principles and Sequence Design, Wiley–Liss, New York, 1999.
[3] H. Geen, R. Freeman, Band-selective radiofrequency pulses, J. Magn. Reson. 93 (1991) 93–141.
[4] L. Emsley, G. Bodenhausen, Optimization of shaped selective pulses for NMR using a quaternion description of their overall propagators, J. Magn. Reson. 97 (1992) 135–148.
[5] E. Kupce, J. Boyd, I.D. Campbell, Short selective pulses for biomedical applications, J. Magn. Reson. Ser. B 106 (1995) 300–303.
[6] H. Lei, J. Peeling, A localized double-quantum filter for in vivo detection of taurine, Magn. Reson. Med. 42 (1999) 454–460.
[7] M. Peres, O. Fedeli, B. Barrere, B. Gillet, G. Berenger, J. Seylaz, J.-C. Beloeil, In vivo identification and monitoring of changes in rat brain glucose by two-dimensional shift correlated ^{1}H NMR spectroscopy, Magn. Reson. Med. 27 (1992) 356–361.
[8] L. Jouvensal, P.G. Carlier, G. Bloch, Practical implementation of single-voxel double-quantum editing on a whole-body NMR spectrometer: localized monitoring of lactate in the human leg during and after exercise, Magn. Reson. Med. 36 (1996) 487–490.
[9] J.R. Keltner, L.L. Wald, B.D. Frederick, P.F. Renshow, In vivo detection of GABA in human brain using a localized double-quantum filter technique, Magn. Reson. Med. 37 (1997) 366–371.
[10] J. Pauly, P. Le Roux, D. Nishimura, A. Macovski, Parameter relations for the Shinnar–Le Roux selective excitation pulse design algorithm, IEEE Trans. Med. Imaging 10 (1991) 53–65.
[11] J. Pauly, D. Spielman, A. Macovski, Echo-planar spin-echo and inversion pulses, Magn. Med. Reson. 29 (1993) 776–782.
[12] F. Schick, Simultaneous highly selective MR water and fat imaging using a simple new type of spectral-spatial excitation, Magn. Reson. Med. 40 (1998) 194–202.
[13] F. Schick, J. Forster, J. Machan, R. Kuntz, C.D. Claussen, Improved clinical echo-planar MRI using spatial-spectral excitation, J. Magn. Reson. Imaging 8 (1998) 960–967.
[14] J.T. Ngo, P.G. Morris, NMR pulse symmetry, J. Magn. Reson. 74 (1987) 122–133.
[15] B. Blumich, H.W. Spiess, Quaternions as a practical tool for the evaluation of composite pulses, J. Magn. Reson. 61 (1985) 356–362.
[16] L.A. Trimble, J.F. Shen, A.H. Wilman, P.S. Allen, Lactate editing by means of selective-pulse filtering of both zero- and double quantum coherence signals, J. Magn. Reson. 86 (1990) 191–198.
[17] J. Shen, D.L. Rothman, P. Brown, In vivo GABA editing using a novel doubly selective multiple quantum filter, Magn. Reson. Med. 47 (2002) 447–454.

[18] P. Blondet, P. Albrand, M. von Kienlin, M. Decorps, N. Lavanchy, Use of rotating-phase DANTE pulses for in vivo proton NMR spectral editing with a single irradiation facility, J. Magn. Reson. 71 (1987) 342–346.
[19] J. Shen, D.C. Shungu, D.L. Rothman, In vivo chemical shift imaging of γ-aminobutyric acid in the human brain, Magn. Reson. Med. 41 (1999) 35–42.
[20] M.A. McLean, A.L. Busza, L.L. Wald, R.J. Simister, G.J. Barker, S.R. Williams, In vivo GABA+ measurement at 1.5 T using a PRESS-localized double quantum filter, Magn. Reson. Med. 48 (2002) 233–241.
[21] L. Emsley, G. Bodenhausen, Phase shifts induced by transient Bloch–Siegert effects in NMR, Chem. Phys. Lett. 168 (1990) 297–303.
[22] C. Bauer, R. Freeman, T. Frenkiel, J. Keeler, A.J. Shaka, Gaussian pulses, J. Magn. Reson. 58 (1984) 442–457.
[23] W.S. Warren, Effects of arbitrary laser or NMR pulse shapes on population inversion and coherence, J. Chem. Phys. 81 (1984) 5437–5448.
[24] A. Knuttel, R. Kimmich, Double quantum filtered volume-selective NMR spectroscopy, Magn. Reson. Med. 10 (1989) 404–410.
[25] D.L. Rothman, O.A.C. Petroff, K.L. Behar, R.H. Mattson, Localized ^{1}H NMR measurement of γ-aminobutyric acid in human brain in vivo, Proc. Natl. Acad. Sci. USA 90 (1993) 5662–5666.
[26] H.P. Hetherington, B.R. Newcomer, J.W. Pan, Measurements of human cerebral GABA at 4.1 T using numerically optimized editing pulses, Magn. Reson. Med. 39 (1998) 6–10.
[27] D.A. Yablonskiy, J.J. Neil, M.E. Raichle, J.J.H. Ackerman, Homonuclear *J* coupling effects in volume localized NMR spectroscopy: pitfalls and solutions, Magn. Reson. Med. 39 (1998) 169–178.
[28] H. Lei, J. Dunn, The effects of slice-selective excitation/refocusing in localized spectral editing with gradient-selected double-quantum coherence transfer, J. Magn. Reson. 150 (2001) 17–25.
[29] J. Shen, R.E. Rycyna, D.L. Rothman, Improvements on an in vivo automatic shimming method (FASTERMAP), Magn. Reson. Med. 38 (1997) 834–839.